Mech Time-Depend Mater (2017) 21:199–221
DOI 10.1007/s11043-016-9326-8

Linear orthotropic viscoelasticity model for fiber reinforced thermoplastic material based on Prony series

Vitor Takashi Endo[1] · **José Carlos de Carvalho Pereira**[2]

Received: 29 April 2016 / Accepted: 13 August 2016 / Published online: 29 September 2016

Abstract Material properties description and understanding are essential aspects when computational solid mechanics is applied to product development. In order to promote injected fiber reinforced thermoplastic materials for structural applications, it is very relevant to develop material characterization procedures, considering mechanical properties variation in terms of fiber orientation and loading time. Therefore, a methodology considering sample manufacturing, mechanical tests and data treatment is described in this study. The mathematical representation of the material properties was solved by a linear viscoelastic constitutive model described by Prony series, which was properly adapted to orthotropic materials. Due to the large number of proposed constitutive model coefficients, a parameter identification method was employed to define mathematical functions. This procedure promoted good correlation among experimental tests, and analytical and numerical creep models. Such results encourage the use of numerical simulations for the development of structural components with the proposed linear viscoelastic orthotropic constitutive model. A case study was presented to illustrate an industrial application of proposed methodology.

Keywords Abaqus CAE · Creep tests · Parameter identification · Prony series · Short fiber reinforced thermoplastic · UMAT Subroutine

1 Introduction

Fiber reinforced thermoplastic materials have received increasing attention in recent years to manufacture structural parts in industry for products with high added value such as vehicles, aircrafts, household appliances, and so on (Masuelli 2013; Tanasa and Zanoaga 2013;

✉ V.T. Endo
endo.takashi@ufsc.br

J.C. de Carvalho Pereira
j.c.carvalho.p@ufsc.br

1 Mobility Engineering Department, Federal University of Santa Catarina, Rua Dr. João Colin, Santo Antônio, 2700, Joinville, SC, Brazil

2 Mechanical Engineering Department, Federal University of Santa Catarina, Campus Universitário, Trindade, Florianópolis, SC, Brazil

Jeyanthi and Rani 2012; Prabhakaran and Kumar 2012; Mertz 2003). The advantages over traditional materials include, among others, high strength-to-weight ratio and high stiffness-to-weight ratio. These characteristics are directly related to structural applications, in terms of materials selection. Additionally, components made of short fiber reinforced thermoplastic materials have relatively low processing costs, especially if the injection molding process is used (Li 2015; Yang et al. 2013; Östergren 2013; Vélez-García et al. 2011; Araújo et al. 2009; Chang and Yang 2001).

According to Banks et al. (2011) and Reese and Govindjee (1998), thermoplastic materials exhibit simultaneously elastic and viscous behavior, which depends on material characteristics and microstructure. Fiber reinforced composite materials show anisotropic properties due to fiber orientation and also viscoelastic behavior due to thermoplastic matrix.

In order to prevent failure modes related to viscoelastic behavior in structural parts made of fiber reinforced thermoplastic materials, an overview of available research was performed. Abadi (2008) showed an implicit finite element method to analyze the thermoforming process of thermoplastic sheets reinforced with unidirectional continuous fibers in which the transient reversible network theory was used to model anisotropic material behavior. Drozdov et al. (2010) derived constitutive equations using finite thermo-viscoelasticity model to describe polymer melting; parameters were adjusted using experimental curve fitting.

In Despringre et al. (2014), a new micromechanical model was used for high cycle fatigue damage of short glass fiber reinforced Polyamide-66. Proposed material model considered damage and nonlinear viscoelasticity matrix.

Nguyen et al. (2007) presented constitutive models considering anisotropy and finite-deformation viscoelasticity, in which fiber and polymeric matrix can exhibit distinct time-dependent behavior. Nedjar (2007) examined a fully three-dimensional constitutive model for anisotropic viscoelasticity, which is suitable for the macroscopic description of fiber reinforced composites that experience finite strains. It was considered that the polymeric matrix and the fibers are treated separately, allowing it to represent as many bundles of fibers as desired. Nedjar (2011) developed a model for the macroscopic description of unidirectional fiber reinforced composites. Fiber contribution was considered as time-independent and linearly elastic, while viscoelastic matrix experiences creep only in shear. In Chevali (2009), an analysis of creep as a function of variables like fiber length, fiber volume fraction and material degradation due to moisture absorption and ultraviolet radiation was performed. Papadogiannis et al. (2009) evaluated the creep behavior and the viscoelastic properties at different temperatures for glass fiber and carbon fiber endodontic posts.

In the work presented by Suchocki (2013), the framework of QLV—Quasi Linear Viscoelastic theory was used to formulate a new rheological model able to capture the nonlinear viscoelastic behavior of thermoplastics and resins. This model was implemented into the FE—Finite Element system of commercial software Abaqus. In Puso and Weiss (1998), a theoretical and computational framework was developed to apply finite element method to anisotropic viscoelastic soft tissues. A discrete spectrum approximation was developed for QLV relaxation function.

Ghazisaeidi (2006) studied the effects of anisotropic material properties of the short glass fiber reinforced thermoplastics on acoustic behavior. Numerical tools were employed to investigate steady dynamic responses of the plastic model under a harmonic excitation. Fiber orientation was obtained using injection molding simulation.

As noted, studies related to material characterization and constitutive models are required to understand viscoelastic behavior of composite parts. These developments, combined with a finite element code, allow a significant improvement of product development process.

Due to the lack of a proper model for linear orthotropic viscoelastic materials in current commercial finite element packages, the aim of this paper is to implement this constitutive

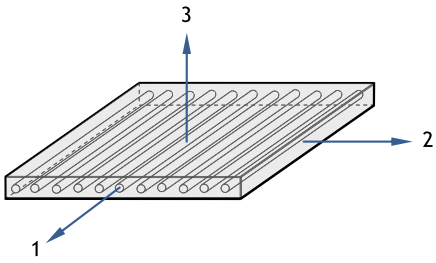

Fig. 1 Fiber orientation

model as a subroutine and identify its Prony series parameters by fitting numerical and experimental creep test data. Considering this numerical tool improvement, it is possible to study particular failure modes related to viscoelastic behavior in composite parts.

2 Materials and methods

This section describes theory and methodology considered to support research regarding experimental procedures, data treatment, constitutive model and user subroutine.

2.1 Linear orthotropic viscoelasticity

It is well established that mechanical properties of fiber reinforced plastics depend on material orientation. Mechanics of composite materials usually describe longitudinal and transverse directions related to fiber, which are described in Fig. 1.

Orthotropic models consider different material behavior for each orthogonally related direction. As a consequence, more parameters are needed to fully describe material behavior when compared to isotropic materials. The stiffness matrix of orthotropic materials showing elastic constants is presented in Eq. (1), where the term Δ is defined in Eq. (2):

$$\begin{Bmatrix} \sigma_1 \\ \sigma_2 \\ \sigma_3 \\ \tau_{12} \\ \tau_{13} \\ \tau_{23} \end{Bmatrix} = \begin{bmatrix} \frac{1-\nu_{23}\nu_{32}}{E_2E_3\Delta} & \frac{\nu_{21}-\nu_{31}\nu_{23}}{E_2E_3\Delta} & \frac{\nu_{31}-\nu_{21}\nu_{32}}{E_2E_3\Delta} & 0 & 0 & 0 \\ \frac{\nu_{12}-\nu_{13}\nu_{32}}{E_3E_1\Delta} & \frac{1-\nu_{31}\nu_{13}}{E_3E_1\Delta} & \frac{\nu_{32}-\nu_{31}\nu_{12}}{E_3E_1\Delta} & 0 & 0 & 0 \\ \frac{\nu_{13}-\nu_{12}\nu_{23}}{E_1E_2\Delta} & \frac{\nu_{23}-\nu_{13}\nu_{21}}{E_1E_2\Delta} & \frac{1-\nu_{12}\nu_{21}}{E_1E_2\Delta} & 0 & 0 & 0 \\ 0 & 0 & 0 & G_{12} & 0 & 0 \\ 0 & 0 & 0 & 0 & G_{13} & 0 \\ 0 & 0 & 0 & 0 & 0 & G_{23} \end{bmatrix} \begin{Bmatrix} \varepsilon_1 \\ \varepsilon_2 \\ \varepsilon_3 \\ \gamma_{12} \\ \gamma_{13} \\ \gamma_{23} \end{Bmatrix}, \tag{1}$$

$$\Delta = \left(\frac{1 - \nu_{12}\nu_{21} - \nu_{23}\nu_{32} - \nu_{31}\nu_{13} - 2\nu_{12}\nu_{23}\nu_{31}}{E_1E_2E_3} \right). \tag{2}$$

It should be noted that the Voigt notation is used through the text due to the symmetric tensors; thus, second-order tensors are presented as column matrices with independent components.

Materials, in general, can exhibit both instantaneous and time-dependent response. As a reference for this representation, classic viscoelasticity models proposed by Kelvin and Maxwell describe a spring and a dashpot for instantaneous and time-dependent properties, respectively.

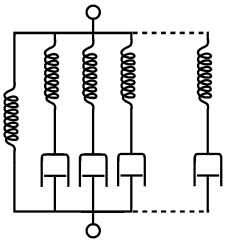

Fig. 2 Representation of generalized Maxwell model

Viscoelasticity behavior is typically observed as two typical phenomena: creep, which describes a increase in strain due to a constant stress state, and stress relaxation, representing a decrease in stress when structure is subjected to a constant strain (Christensen 2003).

Linear viscoelasticity hypothesis assumes that strain increment is linearly proportional to stress, acting as a linear scale factor for creep behavior. This assumption is usually considered valid for small stress levels. Higher stress states or temperatures can induce nonlinear viscoelasticity or even viscoplastic material behavior.

2.2 Constitutive model based on Prony series

Generalized Maxwell model defines a material representation as a parallel combination of n Maxwell's spring–dashpot association, as shown in Fig. 2. The mathematical representation of such idealization is a summation of exponential terms defined as Prony series, as shown in Eq. (3). It should be noted that n also corresponds to the number of summation terms of Prony series, as stated by Park (2001) and Tschoegl (1989).

$$\sum_{i=1}^{n} \alpha_i e^{\frac{-t}{\beta_i}} \tag{3}$$

where

α_i is the first Prony term, and
β_i is the second Prony term.

Commercial FE softwares currently employ Prony series to define time dependency of stress–strain relation in terms of volumetrical and deviatorical stiffness, as written in Eq. (4). It is important to highlight that only isotropic behavior is typically available in FE programs for viscoelasticity models, as also stated by Pettermann and Hüsing (2012).

$$\boldsymbol{\sigma}(t) = \int_0^t K\left(t - t'\right) \frac{d\boldsymbol{\varepsilon_v}}{dt'} dt' + \int_0^t 2G\left(t - t'\right) \frac{d\boldsymbol{\varepsilon_d}}{dt'} dt' \tag{4}$$

where

K is the volumetric stiffness,
G is the deviatoric stiffness,
t is the current time,
t' is the previous time,
$\boldsymbol{\varepsilon_v}$ is the volumetric strain, and
$\boldsymbol{\varepsilon_d}$ is the deviatoric strain.

Based on this representation, volumetrical and deviatorical stiffness are time-dependent functions and are typically represented as Prony series, according to Eqs. (5) and (6), respectively:

$$K(t) = K_{\text{zero}}\left[\alpha_{\infty}^{K} + \sum_{i=1}^{n_K} \alpha_i^K e^{\frac{-t}{\beta_i^K}}\right], \tag{5}$$

$$G(t) = G_{\text{zero}}\left[\alpha_{\infty}^{G} + \sum_{j=1}^{n_G} \alpha_j^G e^{\frac{-t}{\beta_j^G}}\right]. \tag{6}$$

The terms K_{zero} and G_{zero} represent instantaneous material stiffness and are usually obtained from tensile tests. As the variable t approaches zero, Prony series indicates that material stiffness is dictated only by these instantaneous values. Moreover, α_{∞} terms are obtained from Eq. (7), as long as Eq. (8) is satisfied. Each α_i term is related to the loss of stiffness at the time indicated by β_i. Thus, α_{∞} represents residual stiffness when time tends to infinity:

$$\alpha_{\infty} = 1 - \sum_{i=1}^{n} \alpha_i, \tag{7}$$

$$\sum_{i=1}^{n} \alpha_i \leq 1. \tag{8}$$

For the purpose of this work, each elastic term of constitutive model is then formulated to consider a function of time t using Prony series. It is shown in Eq. (9) as a function of elastic modulus for longitudinal fiber direction along time t,

$$E_1(t) = E_{1,\text{zero}}\left[\alpha_{\infty}^{E_1} + \sum_{i=1}^{n_{E_1}} \alpha_i^{E_1} e^{\frac{-t}{\beta_i^{E_1}}}\right]. \tag{9}$$

Elastic modulus in the transverse direction and shear modulus in the transverse plane, written in terms of Prony series, are presented in Eqs. (10) and (11), respectively:

$$E_2(t) = E_{2,\text{zero}}\left[\alpha_{\infty}^{E_2} + \sum_{i=1}^{n_{E_2}} \alpha_i^{E_2} e^{\frac{-t}{\beta_i^{E_2}}}\right], \tag{10}$$

$$G_{12}(t) = G_{12,\text{zero}}\left[\alpha_{\infty}^{G_{12}} + \sum_{i=1}^{n_{G_{12}}} \alpha_i^{G_{12}} e^{\frac{-t}{\beta_i^{G_{12}}}}\right]. \tag{11}$$

Considering that strain values vary along time, i.e., $\varepsilon_x(t)$ and $\varepsilon_y(t)$, it is also expected that Poisson's ratio becomes a function of time, as represented in Eq. (12):

$$\nu_{xy}(t) = \frac{-\varepsilon_y(t)}{\varepsilon_x(t)}. \tag{12}$$

Therefore, Poisson's ratio is also written in terms of Prony series, according to Eqs. (13) and (14). It should be noted that we use the inverse function due to the ascending shape of

Prony series curves:

$$\left(\nu_{12}(t)\right)^{-1} = \nu_{12,\text{zero}}\left[\alpha_{\infty}^{\nu_{12}} + \sum_{i=1}^{n_{\nu_{12}}} \alpha_i^{\nu_{12}} e^{\frac{-t}{\beta_i^{\nu_{12}}}}\right], \tag{13}$$

$$\left(\nu_{21}(t)\right)^{-1} = \nu_{21,\text{zero}}\left[\alpha_{\infty}^{\nu_{21}} + \sum_{i=1}^{n_{\nu_{21}}} \alpha_i^{\nu_{21}} e^{\frac{-t}{\beta_i^{\nu_{21}}}}\right]. \tag{14}$$

Regarding unidirectional fiber composites, it is possible to simplify orthotropic stiffness matrix presented in Eq. (1) as a transversely isotropic material. This assumption considers that directions 2 and 3 of Fig. 1 show the same properties related to transverse fiber orientation. Therefore, elastic parameters as a function of time, indicated in Eqs. (9), (10), (11), (13), and (14), are finally incorporated into the compliance matrix. According to Klasztorny (2008), obtained Eq. (15) can be considered as the coupled standard equation of monotropic viscoelasticity, written using Voigt notation, namely

$$\begin{Bmatrix} \varepsilon_1(t) \\ \varepsilon_2(t) \\ \varepsilon_3(t) \\ \gamma_{12}(t) \\ \gamma_{13}(t) \\ \gamma_{23}(t) \end{Bmatrix} = \begin{bmatrix} \frac{1}{E_1(t)} & \frac{-\nu_{21}(t)}{E_2(t)} & \frac{-\nu_{21}(t)}{E_2(t)} & 0 & 0 & 0 \\ \frac{-\nu_{12}(t)}{E_1(t)} & \frac{1}{E_2(t)} & \frac{-\nu_2}{E_2(t)} & 0 & 0 & 0 \\ \frac{-\nu_{12}(t)}{E_1(t)} & \frac{-\nu_2}{E_2(t)} & \frac{1}{E_2(t)} & 0 & 0 & 0 \\ 0 & 0 & 0 & \frac{1}{G_{12}(t)} & 0 & 0 \\ 0 & 0 & 0 & 0 & \frac{1}{G_{12}(t)} & 0 \\ 0 & 0 & 0 & 0 & 0 & \frac{2(1+\nu_2)}{E_2(t)} \end{bmatrix} \begin{Bmatrix} \sigma_1(t) \\ \sigma_2(t) \\ \sigma_3(t) \\ \tau_{12}(t) \\ \tau_{13}(t) \\ \tau_{23}(t) \end{Bmatrix}. \tag{15}$$

2.3 Experimental procedures

Material characterization procedures were conducted to identify mechanical properties of polybutylene terephthalate (PBT) with 20 % content of glass fiber (GF) reinforcement.

Samples for tensile tests are usually obtained from a mold cavity with dimensions indicated by standards. Arjmand et al. (2011) shows schematics of a dog-bone sample obtained directly from injection molding. This procedure becomes limited to isotropic materials, as only one direction can be evaluated. Therefore, it is not suitable for characterization of fiber reinforced materials.

Based on this drawback, an injected plate is proposed to provide samples with different fiber orientation. It is noteworthy that this injected plate was developed previously and its intent was to get uniform region in terms of fiber orientation. Rios (2012) performed an injection molding simulation and indicated that the square region of plate tends to present a uniform distribution.

Assuming that main region of plate presents uniform fiber orientation, samples were finally cut accordingly to 0°, 90° and 45°, as shown in Fig. 3. Dimensions were consistent with ANSI/ASTM D638 and ANSI/ASTM D2990 standards.

The waterjet cutting technique was employed to obtain samples in order to prevent polymer degradation during this process. It should be pointed out that degradation was observed in previous attempts using laser cutting. The fiber orientation angle of samples θ, defining local $(1, 2, 3)$ and global (x, y, z) coordinate system, is illustrated in Fig. 4.

In order to capture longitudinal and transverse strains in time, strain gauges were attached on a sample and a dummy, as shown in Fig. 5. It is important to emphasize that a

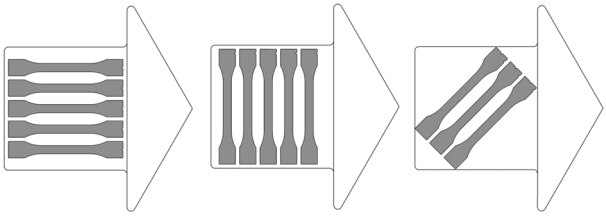

Fig. 3 Injected plate

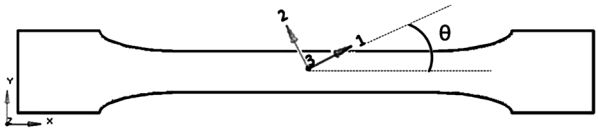

Fig. 4 Fiber orientation angle

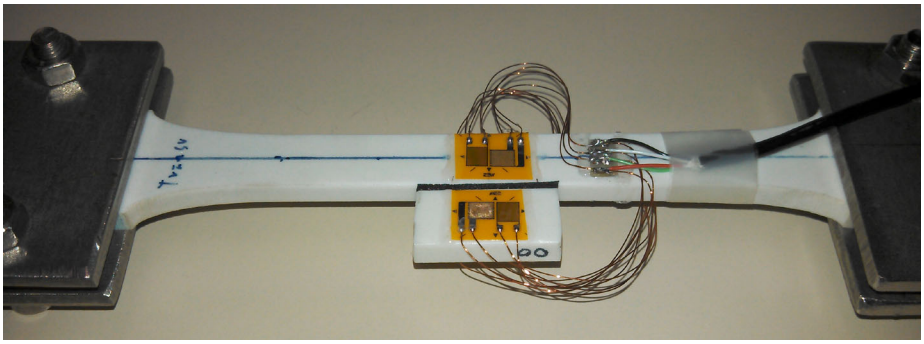

Fig. 5 Strain gauge and a dummy

Table 1 Load of creep test for each sample orientation

Orientation	Load (N)	Area (mm^2)	Stress (MPa)
0°	468.15	38.06	12.30
90°	467.17	39.28	11.89
45°	472.02	38.88	12.14

Wheatstone full-bridge configuration was applied in order to prevent eventual thermally related strain measures, as indicated by Rosa (2004) and Malerba et al. (2008). We also wish to highlight the fact that the fiber orientation of the dummy is consistent with the sample. Strain measurements were then stored using data acquisition system HBM Spider 8.

Samples were subjected to tensile tests with prescribed displacement ratio of 5 mm/min, as indicated by standards. The duration of each experiment was less than 35 s. Finally, a maximum stress state of 10 MPa was considered as a stopping criterion.

Additionally, creep tests were conducted to study viscoelastic behavior. In this experiment, a constant stress state is applied and strain is measured in time. Samples were loaded according to Table 1 during approximately 3.5 weeks at a temperature of 23.5 °C. A small value of stress state, when compared to yield stress, is intended to preserve linear viscolasticity assumptions.

2.4 Data treatment

Experimental data of strain values at various times are converted to time-dependent elastic parameters. Elastic moduli (Eqs. (16) and (17)) and Poisson's ratios (Eqs. (18) and (19)) are obtained from strain values of samples with 0° and 90° fiber orientation, while shear modulus is identified from results of sample with 45° fiber orientation:

$$E_1(t) = \frac{\sigma_{x,0^\circ}}{\varepsilon_{x,0^\circ}(t)}, \tag{16}$$

$$E_2(t) = \frac{\sigma_{x,90^\circ}}{\varepsilon_{x,90^\circ}(t)}, \tag{17}$$

$$\nu_{12}(t) = \frac{\varepsilon_{y,0^\circ}(t)}{\varepsilon_{x,0^\circ}(t)}, \tag{18}$$

$$\nu_{21}(t) = \frac{\varepsilon_{y,90^\circ}(t)}{\varepsilon_{x,90^\circ}(t)}. \tag{19}$$

Shear modulus $G_{12}(t)$ can be written in terms of longitudinal or transverse strain, as described in Eqs. (20) and (21), respectively. As strain values in both longitudinal and transverse directions were collected for the 45° sample, final shear modulus is obtained by taking the average of both measures, as indicated in Eq. (22):

$$G_{12,\varepsilon_x}(t) = \frac{\cos^2(\theta)\sin^2(\theta)}{\left(\frac{\varepsilon_{x,45^\circ}(t)}{\sigma_{x,45^\circ}} - \frac{\cos^4(\theta)}{E_1(t)} - \frac{\sin^4(\theta)}{E_2(t)} + \frac{2\nu_{12}(t)\cos^2(\theta)\sin^2(\theta)}{E_1(t)}\right)}, \tag{20}$$

$$G_{12,\varepsilon_y}(t) = \frac{\cos^2(\theta)\sin^2(\theta)}{\left(\frac{\varepsilon_{y,45^\circ}(t)}{\sigma_{x,45^\circ}} - \frac{\cos^2(\theta)\sin^2(\theta)}{E_1(t)} - \frac{\cos^2(\theta)\sin^2(\theta)}{E_2(t)} + \frac{2\nu_{12}(t)\cos^4(\theta)\sin^4(\theta)}{E_2(t)}\right)}, \tag{21}$$

$$G_{12}(t) = \frac{G_{12,\varepsilon_x}(t) + G_{12,\varepsilon_y}(t)}{2}. \tag{22}$$

The value of Poisson ratio of polymer matrix $\nu_2 = 0.44$ was considered constant in time, and it was obtained from manufacturer's material data sheet. This information is necessary to define $G_{23}(t)$, as given in Eq. (23):

$$G_{23}(t) = \frac{E_2(t)}{2(1+\nu_2)}. \tag{23}$$

2.5 Parameter identification

In order to introduce such material models in a structural analysis, it is important to identify mechanical properties in both longitudinal and transverse directions by performing tests and data treatment. However, the proposed model shows a large number of parameters to describe viscoelastic behavior in different directions.

In this regard, material characterization is aided by numerical models and proper optimization techniques. This so-called parameter identification method consists in finding the material coefficients by minimizing the difference between experimental and numerical curves of the same experiment. This procedure is specially useful to characterize nonlinear materials, as studied by Khalfallah et al. (2015) and Vaz et al. (2015).

Table 2 FE programs used in this work

Ansys	Abaqus	Moldflow
Parameter identification	Structural analysis with UMAT	Injection molding

Table 3 Initial values of β_i

β_1	β_2	β_3	β_4	β_5	β_6	β_7
2×10^0	2×10^1	2×10^2	2×10^3	2×10^4	2×10^5	2×10^6

For the purpose of this work, a parameter identification tool already implemented in Ansys was employed. Even though it is initially intended for a linear isotropic viscoelastic model, the curve fit algorithm could also be used to find Prony terms of the proposed orthotropic model. As different FE programs were used in the research, Table 2 explains which Computer Aided Engineering (CAE) program was utilized for each task.

A very useful documentation to describe this Ansys feature was written by Imaoka (2008), which recommends to stipulate initial values for β_i, depending on magnitude order of time of creep test. Initial values for these Prony terms, presented in Table 3, allowed convergence in the optimization process with residual values as low as 1×10^{-5}.

2.6 UMAT—user material subroutine

Commercial FE softwares, like Abaqus, allow users and researchers to create their own material model by writing a Fortran code with a proper stress–strain relation that defines a constitutive model. User material subroutines are extensively used to evaluate different material behavior from those already implemented in Abaqus.

During the iterative trial solution, this external subroutine updates stress state based on strain values, and force equilibrium is checked as described by Wang et al. (2012).

Luo and Lee (2008) evaluated damage of Carbon-Epoxy structures using UMAT. Kim et al. (2013) developed a constitutive model to represent viscoplastic damage of austenitic stainless steel. Both Abaqus subroutine studies showed good agreement between experimental and numerical data, indicating the adequacy of material model and user subroutine implementation procedures.

Implementation of constitutive model allows the evaluation of distinct failure modes of materials, improving numerical simulation capabilities to solve engineering problems. In this context, linear orthotropic viscoelastic model can be applied to evaluate short fiber reinforced composites, manufactured by injection molding process. This model can predict nodal displacement along time of a structure when it is subjected to a constant load.

It is particularly noteworthy that time t, which is a variable of constitutive model, was represented by the time step value of FE program. Furthermore, material orientation was applied using graphical interface of Abaqus.

The success of subroutine implementation can be checked by running a numerical creep test with same parameters as the analytic model. Outputs like strain variation in time in both longitudinal and transverse direction are compared. This verification is very important due to the inherent complexity of programming process and its data transfer to finite element solver.

Finally, once the subroutine is properly implemented, it is possible to apply such a material model to an arbitrary geometry, making use of all FE benefits in terms of the CAE tool in a product development context.

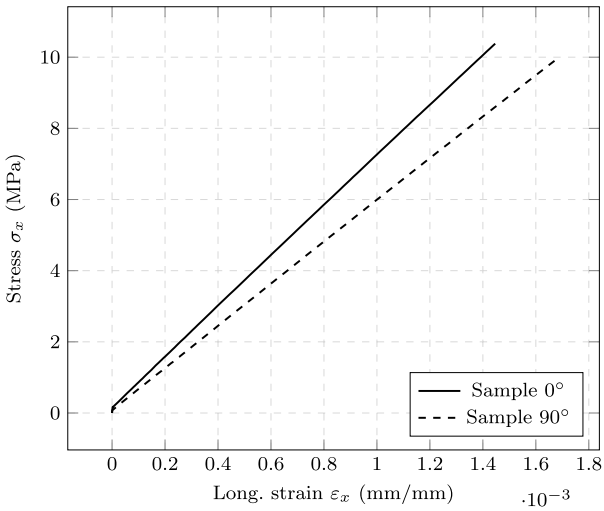

Fig. 6 Tensile test: elastic moduli E_1 and E_2

3 Results

In this section, expected results are related to experimental procedures of tensile and creep tests, optimization results of parameter identification method, and finally numerical results of subroutine implementation.

3.1 Tensile test

Material stiffness is characterized using averaged stress vs strain curves from tensile tests, as shown in Fig. 6. As a consequence of fiber orientation, it was found that 0° fiber orientation samples are stiffer when compared to those with 90° fiber orientation.

Poisson's ratio is defined by the negative ratio of transverse to longitudinal strain. As seen in Fig. 7, ν_{12} and ν_{21} are observed as the slopes of a line, considering samples with 0° and 90° of fiber orientation, respectively. Based on that experiment, it was found that $\nu_{21} = 0.2948$; however, in order to ensure the symmetry of compliance matrix, ν_{21} was obtained using Eq. (24). Either way, that symmetry is numerically imposed during the solution for proper representation of orthotropy model:

$$\nu_{21} = \frac{E_2 \nu_{12}}{E_1}. \tag{24}$$

Note that shear stiffness is identified with 45° fiber orientation samples, as also mentioned by Yokoyama and Nakai (2007). As it can be seen in Eqs. (25) and (26), shear stress and shear strain can be obtained from experimental data. This procedure is important because, as noted earlier, experimental data are in the global coordinate system (x, y, z):

$$\tau_{12} = \frac{\sigma_{x,45^\circ}}{2}, \tag{25}$$

$$\gamma_{12} = \varepsilon_{x,45^\circ} - \varepsilon_{y,45^\circ}. \tag{26}$$

Finally, the definition of shear modulus is shown in Eq. (27),

$$G_{12} = \frac{\tau_{12}}{\gamma_{12}}. \tag{27}$$

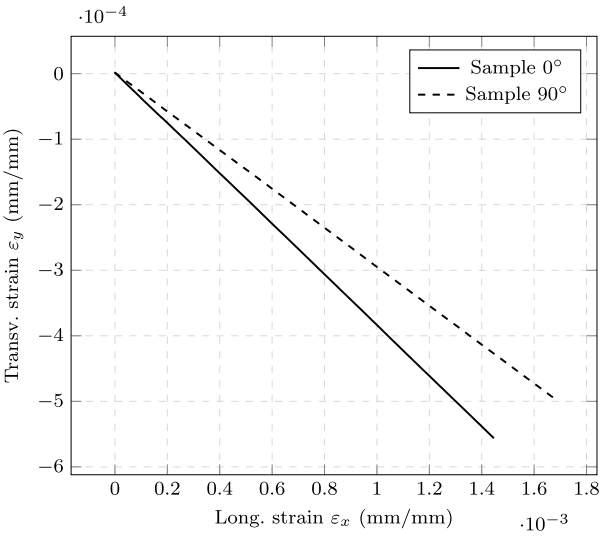

Fig. 7 Tensile test: Poisson's ratios ν_{12} and ν_{21}

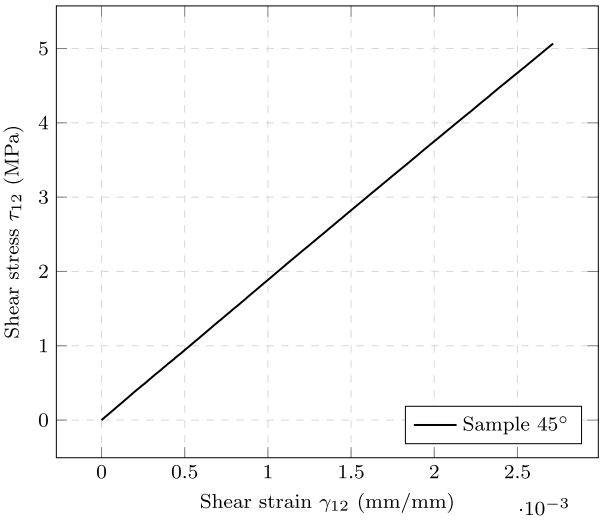

Fig. 8 Tensile test: shear modulus G_{12}

As shown in Fig. 8, shear modulus G_{12} is identified as the slope of the line relating shear stress and engineering shear strain.

As presented previously by Sonnenhohl (2012), the yield stress of Ticona Celanex 3226 was determined in the longitudinal and transverse directions as $\sigma_{\text{yield},1}$ and $\sigma_{\text{yield},2}$, respectively. Finally, these so-called instantaneous properties obtained from tensile test are then summarized in Table 4.

3.2 Creep test

The results of creep tests are presented in terms of strain values varying in time. The results in longitudinal and transverse direction are presented in Figs. 9 and 10, respectively.

Table 4 Elastic properties obtained from tensile test

E_1 (MPa)	E_2 (MPa)	G_{12} (MPa)	ν_{12}	ν_{21}	$\sigma_{\text{yield},1}$ (MPa)	$\sigma_{\text{yield},2}$ (MPa)
7178.4	5976.0	1874.6	0.3836	0.3193	52.36	41.54

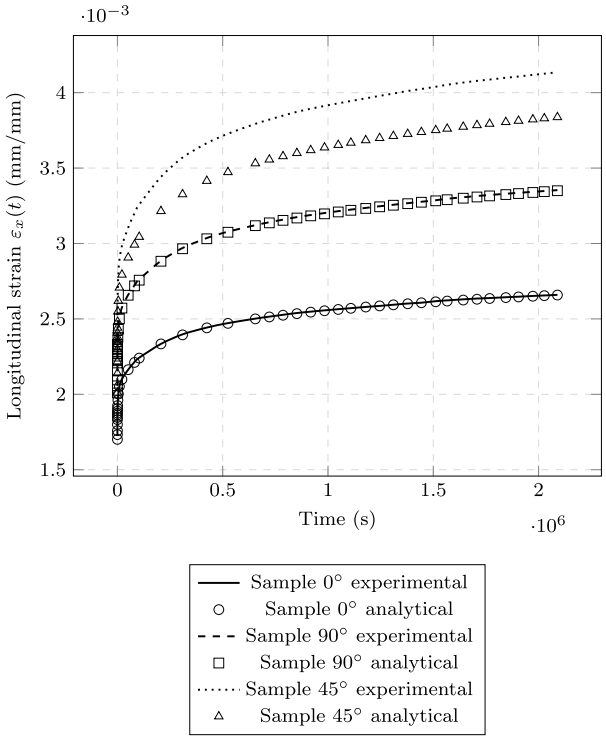

Fig. 9 Creep test: longitudinal strain

3.3 Parameter identification

Experimental strain data were converted to time-dependent elastic parameters as proposed earlier. Using the parameter identification methodology, the unknowns of orthotropic viscoelastic constitutive model can be properly specified. The Prony series parameters of elastic modulus, shear modulus and Poisson's ratio are finally presented in Tables 5, 6 and 7, respectively. It should be noted that a large number of coefficients are needed for each material property, as a consequence of a constitutive model using 7 Prony terms. Previous tests using fewer Prony terms indicated poor material representation; this finding is corroborated by Imaoka (2008), who described a recommendation regarding the number of Prony terms as dependent on the magnitude order of the total time of creep test experiment.

In order to verify obtained parameters, curves of material properties varying in time are plotted comparing experimental and analytical data. Elastic modulus, shear modulus and Poisson's ratio are illustrated in Figs. 11, 12 and 13, respectively.

Good agreement between experimental and analytical curves was found, highlighting the fact that analytical ones employed Prony parameters obtained earlier. As can be seen in Table 8, consistent values were found for most elastic parameters obtained from tensile

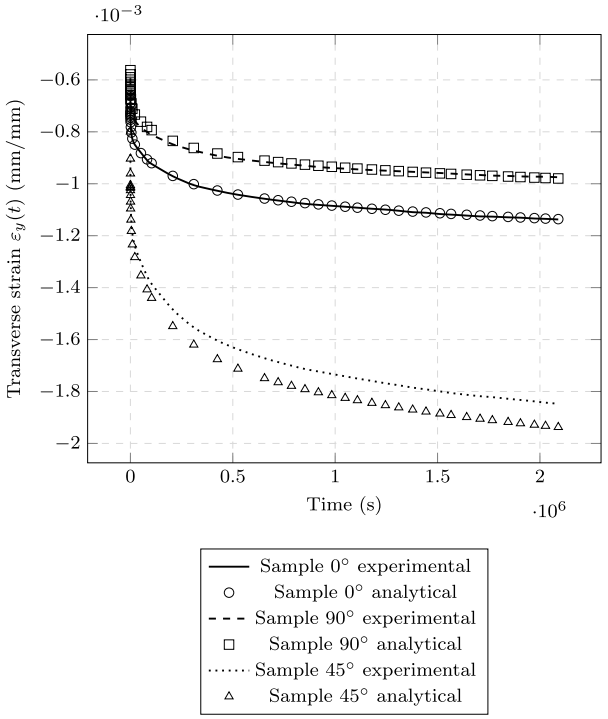

Fig. 10 Creep test: transverse strain

Table 5 Polybutylene terephthalate (20 % content of glass fiber): elastic modulus

i	$E_1(t)$		$E_2(t)$	
	$E_{1,\text{zero}}$	$\alpha_\infty^{E_1}$	$E_{2,\text{zero}}$	$\alpha_\infty^{E_2}$
	7230	0.61821	5920	0.57300
	$\alpha_i^{E_1}$	$\beta_i^{E_1}$	$\alpha_i^{E_2}$	$\beta_i^{E_2}$
1	1.4×10^{-8}	6.068×10^{0}	1.7×10^{-8}	1.611×10^{2}
2	0.081056	4.063×10^{1}	0.106020	4.171×10^{1}
3	0.021855	4.829×10^{2}	0.027796	9.609×10^{2}
4	0.062266	3.996×10^{3}	0.061810	5.299×10^{3}
5	0.031572	4.066×10^{4}	0.033271	4.285×10^{4}
6	0.089900	1.785×10^{5}	0.094028	1.963×10^{5}
7	0.095136	1.419×10^{6}	0.104070	1.536×10^{6}

and creep tests. Based on the creep test, it was found that $\nu_{21} = 0.2801$; however, in order to ensure symmetry of the compliance matrix, ν_{21} was obtained using Eq. (24). Therefore, instantaneous Poisson's ratio should be modified to $\nu_{23,\text{zero}} = 3.14$.

3.4 Numerical simulation

As the constitutive model is implemented in a commercial FE program, a numerical creep test was conducted employing identified material parameters. Therefore, a solid mesh model

Table 6 Polybutylene terephthalate (20 % content of glass fiber): shear modulus

i	$G_{12}(t)$		$G_{23}(t)$	
	$G_{12,\text{zero}}$	$\alpha_\infty^{G_{12}}$	$G_{23,\text{zero}}$	$\alpha_\infty^{G_{23}}$
	2160	0.46507	2055	0.57300
	$\alpha_i^{G_{12}}$	$\beta_i^{G_{12}}$	$\alpha_i^{G_{23}}$	$\beta_i^{G_{23}}$
1	0.000270	0.160×10^{0}	4.8×10^{-8}	5.312×10^{3}
2	0.154200	1.500×10^{1}	0.106020	4.171×10^{1}
3	0.047641	5.615×10^{2}	0.027796	9.609×10^{2}
4	0.078885	4.142×10^{3}	0.061810	5.299×10^{3}
5	0.042497	4.305×10^{4}	0.033271	4.285×10^{4}
6	0.106050	1.840×10^{5}	0.094028	1.963×10^{5}
7	0.105390	1.317×10^{6}	0.104070	1.536×10^{6}

Table 7 Polybutylene terephthalate (20 % content of glass fiber): Poisson's ratios

i	$(\nu_{12}(t))^{-1}$		$(\nu_{21}(t))^{-1}$	
	$\nu_{12,\text{zero}}$	$\alpha_\infty^{\nu_{12}}$	$\nu_{23,\text{zero}}$	$\alpha_\infty^{\nu_{23}}$
	2.57	0.90194	3.57	0.95785
	$\alpha_i^{\nu_{12}}$	$\beta_i^{\nu_{12}}$	$\alpha_i^{\nu_{23}}$	$\beta_i^{\nu_{23}}$
1	0.008100	7.628×10^{0}	5.4×10^{-3}	0.917×10^{0}
2	2.2×10^{-8}	1.858×10^{1}	3.1×10^{-103}	1.995×10^{1}
3	0.001737	2.081×10^{2}	4.3×10^{-13}	2.000×10^{2}
4	0.019295	1.982×10^{3}	0.007505	2.000×10^{3}
5	0.008047	2.000×10^{4}	0.003491	2.000×10^{4}
6	0.037233	2.000×10^{5}	0.025773	2.000×10^{5}
7	0.023668	2.000×10^{6}	0.000000	2.000×10^{6}

Table 8 Properties obtained from tensile and creep test

	Tensile test	Creep test	
E_1 (MPa)	7178	7230	−0.72%
E_2 (MPa)	5976	5920	0.94%
G_{12} (MPa)	1875	2160	−15.20%
ν_{12}	0.3836	0.3891	−1.43%
ν_{21}	0.3193	0.3185	0.25%

representing the test sample subjected to constant stress state according to Table 1 was evaluated in time.

Strain values in both longitudinal and transverse directions were recorded from simulation and presented to be compared to analytical ones. The creep test results of samples with fiber orientation angle of 0°, 90° and 45° are shown in Figs. 14, 15 and 16, respectively. These comparative results indicated that the subroutine implementation was performed successfully.

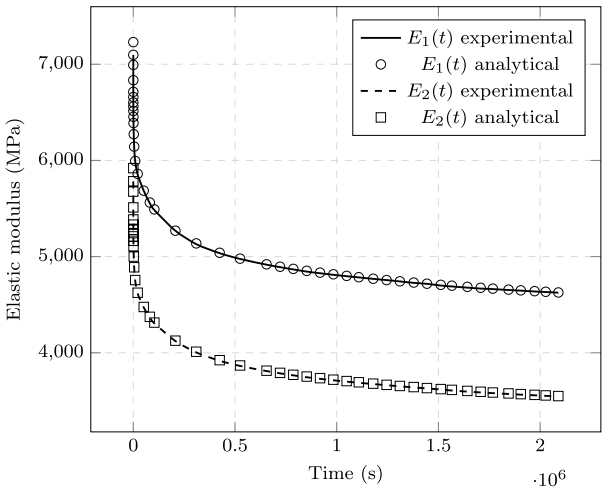

Fig. 11 Parameter identification results: elastic modulus

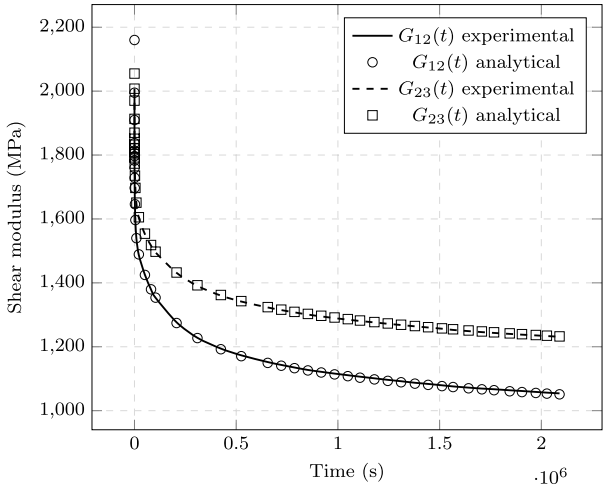

Fig. 12 Parameter identification results: shear modulus

3.5 Industrial application: injection molding and structural simulation

Considering that the material subroutine was properly implemented in a commercial FE program, it is possible to apply such a constitutive model to perform structural analysis of a product. In other words, this methodology allows engineers to check failure modes related to viscoelastic behavior. For instance, for some applications it might be interesting to predict and evaluate displacement over time in a fiber reinforced product subjected to constant load. It is important to highlight the fact that stress state is compatible with linear viscoelastic behavior, otherwise simulation would provide misleading results.

A case study is presented in this section to exemplify an industrial application of the methodology presented in this paper. The fiber orientation was obtained via an injection molding simulation, and this information was imported into a structural finite element program using solid mesh. As mechanical properties are functions of fiber orientation, it is important to perform a manufacturing process simulation and then import such data to struc-

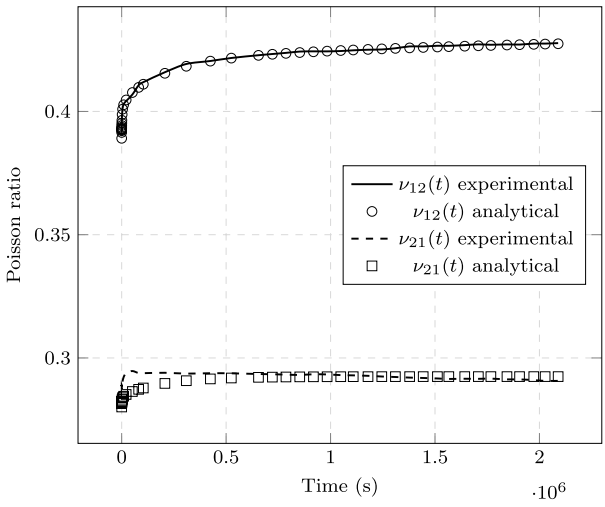

Fig. 13 Parameter identification results: Poisson's ratio

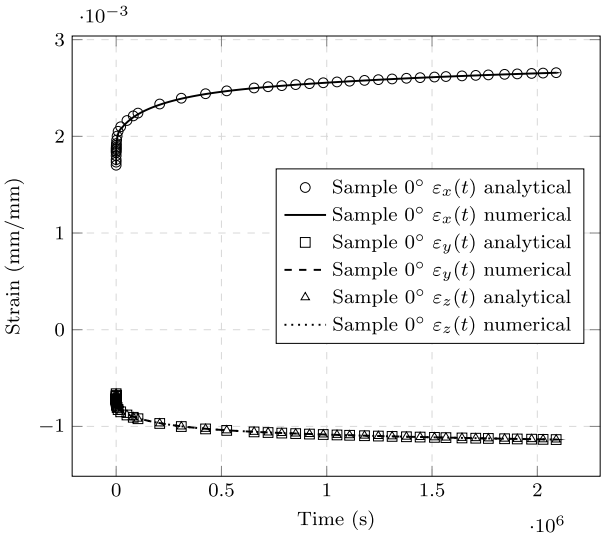

Fig. 14 Strain variation in time: sample with $\theta = 0°$

tural analysis. This is an analogous procedure to that when considering residual stresses due to the forming process in a sheet metal part.

Fiber orientation is a result of the filling stage of the injection process which can be evaluated using numerical tools. Moldflow simulation indicates a prediction of fiber orientation due to the filling stage of injection molding, as presented in Fig. 17. According to Moldflow documentation and Chung et al. (2002), the fiber orientation tensor measures the proportion of fiber alignment in a specified direction.

This simulation result also indicates welding lines which are formed when two flow fronts meet head on (Shoemaker 2006). It can be considered unavoidable in parts with holes or multigated injection concept. It is important to highlight that mechanical properties are locally reduced at these locations. Ozcelik et al. (2012) studied a methodology to evaluate the effects of injection parameters on the welding line tensile strength.

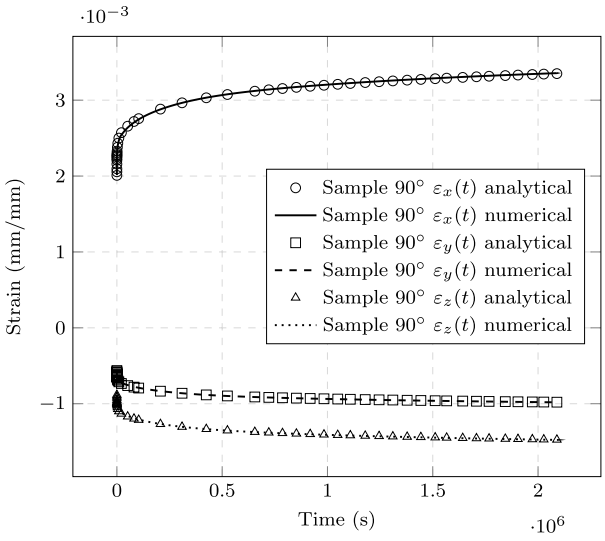

Fig. 15 Strain variation in time: sample with $\theta = 90°$

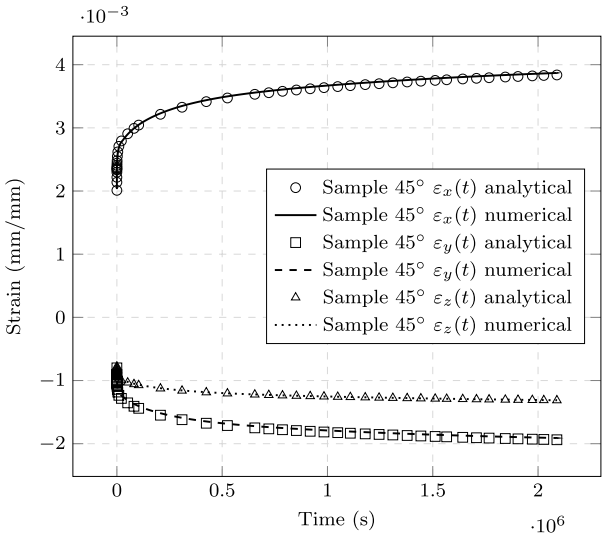

Fig. 16 Strain variation in time: sample with $\theta = 45°$

Information regarding fiber orientation was imported in Abaqus using a Moldflow script program to convert such information. Material orientation of elements is presented in Fig. 18.

As a consequence of constant flexural load applied on the structure, a stress state can be obtained. As shown in Fig. 19, higher values are observed next to stress concentrators. Evaluated stress component is aligned with longitudinal direction of fibers. It is noteworthy that this stress state is in the range of creep test.

A vertical displacement plot is presented in Fig. 20, showing fixed and free edges of the structure. Due to viscoelastic behavior, vertical displacement tends to increase in time. This may lead to a component failure depending on the particular product requirements.

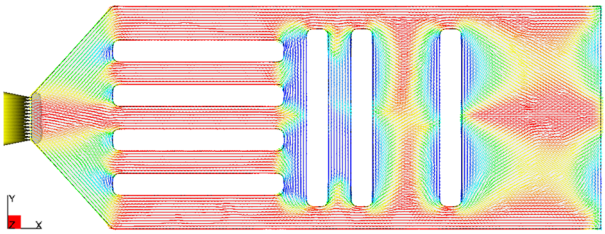

Fig. 17 Moldflow result: fiber orientation due to injection process in the x-direction

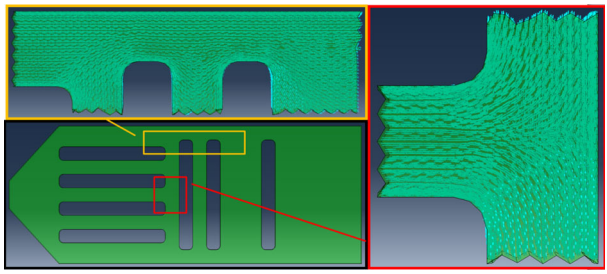

Fig. 18 Fiber orientation imported in Abaqus

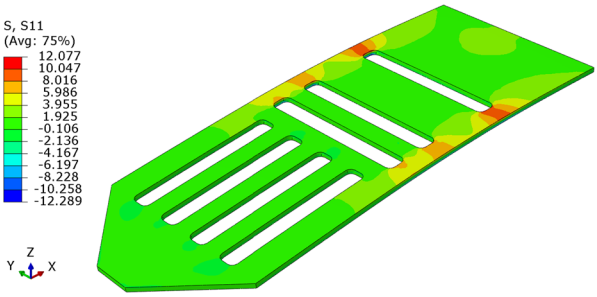

Fig. 19 Abaqus result: stress in longitudinal fiber direction (MPa)

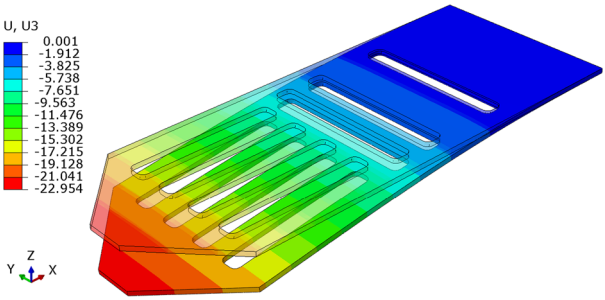

Fig. 20 Abaqus result: vertical displacement (mm)

Based on results of converged substeps, a curve showing displacement in time can be demonstrated in Fig. 21. This information could be used to identify required time to achieve failure considering this mechanical load. Instantaneous displacement is observed at the first point of the curve with value of 13.9 mm; after 2×10^6 s, displacement reached 22.9 mm.

This case study using proposed constitutive model shows how numerical tools could improve mechanical design of a structure. Integration of manufacturing and structural simu-

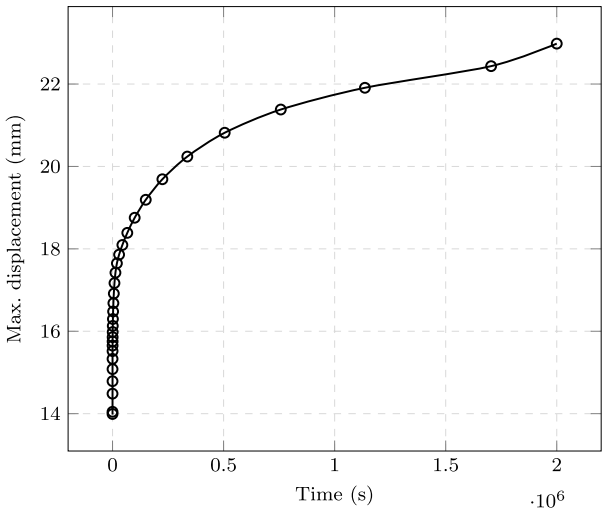

Fig. 21 Displacement variation in time

lation results leads to significant improvements on numerical models and allows for product development of composite structures using virtual prototypes.

4 Discussion

This study aimed to describe the implementation of a linear orthotropic viscoelasticity constitutive model, in order to simulate composite structures. Procedures related to material characterization, mathematical model, parameter identification and subroutine implementation were presented.

We found that parameter identification is a good strategy to characterize viscoelastic behavior of composite materials, due to the large number of unknowns of proposed constitutive model. This procedure saved time and provided good results, as confirmed by comparative curves presenting analytical and experimental data. Although there are other mathematical functions that could drastically reduce the number of material parameters needed for time-dependency of material properties, Prony series were adopted in this work due to the analogy of isotropic material model implemented in current FE programs. Thus, due to this drawback related to the large number of coefficients, future work could evaluate the use of fractional exponential function for viscoelastic materials, indicating its analytical inversion of constitutive equation.

It is important to remark that, due to the stress calculation using Eq. (15), proposed user subroutine is restricted to external loads defined by the Heaviside step function. Further work could develop a general material model using a convolution integral form in order to enable arbitrary load cases.

In regards to identified material parameters for longitudinal and transverse directions, an interesting fact was observed for Prony series terms. Similar values of α_i were obtained for elastic and shear moduli, remembering that this parameter is related to the loss of stiffness at the time defined by β_i. One should notice that instantaneous properties basically differentiate each property. This observation agrees with the fact that fiber phase, which contains elastic glass material, implies different instantaneous properties according to fiber orientation. On the other hand, the matrix phase, which contains thermoplastic material, is strongly

related to viscoelastic behavior. Thus, instantaneous behavior is a fiber-dominant property while time-dependent behavior is a matrix-dominant property. As α_i terms do not depend on material orientation, viscoelastic characterization might be simplified; characterization of mechanical properties involves a typical creep test taking several days and, depending on test device availability for simultaneous data acquisition, this procedure could simplify material characterization process. This study suggests that viscoelastic characterization of fiber reinforced materials could be optimized considering tensile tests in three fiber orientation angles and one creep test considering any fiber orientation in order to describe instantaneous and time-dependent properties, respectively. Therefore, based on these findings it seems reasonable to modify our approach to characterize time-dependent variables of the proposed constitutive model.

According to Abaqus/Standard 6.14 Documentation, a viscoelastic model available in the material library must be combined with an elastic material model. Additionally, the elasticity for time domain viscoelasticity must be defined by isotropic linear elastic, isotropic hyperelastic or anisotropic hyperelastic material. Based on this statement, it is possible to model orthotropic viscoelasticity by combining viscoelastic and hyperelastic models based on strain energy functions. In this case, volumetric and deviatoric behavior of viscoelasticity are assumed in the form of Prony series. It is also shown in Abaqus' user guide that anisotropic linear elasticity can be used with viscoelastic material in Abaqus/Explicit version. The proposed linear viscoelastic model using UMAT considered orthotropic elastic behavior during implicit solution of Abaqus/Standard. Once this constitutive model allows evaluation of failure modes related to constant load, it presents a significant improvement for numerical analysis of composite structures.

The results regarding Poisson ratio along time were similar to those of Pandini and Pegoretti (2008) and Tschoegl et al. (2002), showing that this parameter tends to increase in time. These authors also emphasize the influence of temperature as well.

It was expected that shear modulus would be the same for longitudinal and transverse strain data, as stated by Eqs. (20) and (21). Due to the lack of relation between those curves, an average curve was assumed. As a result, neither longitudinal nor transverse strain could properly represent the creep test results for the sample with 45° of fiber orientation, as presented in Figs. 9 and 10. We propose the lack of a strong alignment in that direction as a possible explanation of this fact.

The obtained parameters of the constitutive model for this particular material may be viewed with caution due to small sample size available for this study. These parameters are valid for a specific production batch, as it is well established that injection parameters can affect mechanical properties of the samples. Moreover, some implications of the findings of this work may not be generalized to a broader range of stress state. This constitutive model, as a consequence of linear viscoelasticity assumption, is more representative if the stress level is comparable to those of the creep test. So one must check if the stress level and environmental variables such as temperature allow this linear behavior.

More experimental studies are important to check the limits of linear viscoelasticity assumption, by performing creep tests with increasing load values. Isochronous curves should be constructed for the tested material, in order to identify the strain range of linear viscoelastic behavior.

Finally, further studies will be necessary to understand how the parameters of manufacturing process, like gate design, packing, mold temperature, cooling system and part thickness can modify mechanical properties. In regards to future research, temperature dependency will be important to complement linear orthtropic viscoelasticity and viscoplasticity models using Prony series.

Despite the minor limits of this study, we believe our findings may contribute to improve mechanical design of composite materials using numerical tools, by describing a comprehensive methodology concerning the proposed constitutive model. A case study of a hypothetical structure subjected to a constant load was performed using proposed material model, in which fiber orientation of each element was obtained by injection molding simulation. This exemplifies a methodology to evaluate viscoelasticity failure modes of composite parts. Thus, this study may contribute to innovations in the field of short fiber composite structures.

Introducing composite materials to industry brings many mechanical design and manufacturing challenges. Therefore, such developments of numerical tools to evaluate structures considering manufacturing process play an important role to material substitution in an industrial context. We hope that this work could contribute to disseminate information related to injected composite parts and their applications.

Acknowledgements We wish to thank Professors Lauro Cesar Nicolazzi, Gean Vitor Salmoria and Guilherme Mariz de Oliveira Barra for their careful reading and feedback on the study. We also want to thank Luiz Carlos Pinagé de Lima Filho for providing valuable samples and Armin Sonnenhohl for conducting mechanical tests at laboratory. Finally, we wish to thank funding and support of CAPES (Coordination of Improvement of Higher Education Personnel).

References

Abadi, M.T.: Viscoelastic model for thermoforming process of thermoplastic composite sheets. In: 9th International Conference on Flow Processes in Composite Materials, vol. 6, Montreal, Canada, 07.07 (2008)

Araújo, B.J., Teixeira, J.C.F., Cunha, A.M., Groth, C.P.T.: Parallel three-dimensional simulation of the injection molding process. Int. J. Numer. Methods Fluids **59**(7), 801–815 (2009). doi:10.1002/fld.1852

Arjmand, M., Mahmoodi, M., Gelves, G.A., Park, S., Sundararaj, U.: Electrical and electromagnetic interference shielding properties of flow-induced oriented carbon nanotubes in polycarbonate. Carbon **49**(11), 3430–3440 (2011). http://www.sciencedirect.com/science/article/pii/S0008622311003034. doi:10.1016/j.carbon.2011.04.039

Banks, H.T., Hu, S., Kenz, Z.R.: A brief review of elasticity and viscoelasticity for solids. Adv. Appl. Math. Mech. **3**, 1–51 (2011). http://journals.cambridge.org/article_S207007330000151X. doi:10.4208/aamm.10-m1030

Chang, R.y., Yang, W.h.: Numerical simulation of mold filling in injection molding using a three-dimensional finite volume approach. Int. J. Numer. Methods Fluids **37**(2), 125–148 (2001)

Chevali, V.S.: Flexural creep of long fiber thermoplastic composites: effect of constituents and variables on viscoelasticity. Dissertation, University of Alabama at Birmingham (2009)

Christensen, R.: Theory of Viscoelasticity. Civil, Mechanical and Other Engineering Series. Dover, New York (2003). https://books.google.com.br/books?id=_tnm0cMWSNIC

Chung, D.H., Kwon, T.H., et al.: Fiber orientation in the processing of polymer composites. Korea–Aust. Rheol. J. **14**(4), 175–188 (2002)

Despringre, N., Chemisky, Y., Arif, M.F., Robert, G., Meraghni, F.: Multi-scale viscoelastic damage model of short glass fiber reinforced thermoplastics under fatigue loading. In: 16th European Conference on Composite Materials, ECCM16 (2014), 8 p.

Drozdov, A., Jensen, E., Christiansen, J.: Nonlinear viscoelastic response of thermoplastic-elastomer melts. Adv. Appl. Math. Mech. **2**(1), 1–31 (2010). doi:10.4208/aamm.09-m0938, 3181

Ghazisaeidi, H.: A description of the anisotropic material behaviour of short glass fibre reinforced thermoplastics using fea. Dissertation, Blenkinge Institute of Technology (2006)

Imaoka, S.: Viscoelasticity. ANSYS Release: 110 (2008). http://ansys.net/collection/1113

Jeyanthi, S., Rani, J.J.: Improving mechanical properties by kenaf natural long fiber reinforced composite for automotive structures. J. Appl. Sci. Eng. **15**(3), 275–280 (2012)

Khalfallah, A., Oliveira, M.C., Alves, J.L., Zribi, T., Belhadjsalah, H., Menezes, L.F.: Mechanical characterization and constitutive parameter identification of anisotropic tubular materials for hydroforming applications. Int. J. Mech. Sci. **104**, 91–103 (2015). http://www.sciencedirect.com/science/article/pii/S0020740315003446. doi:10.1016/j.ijmecsci.2015.09.017

Kim, J.H., Lee, C.S., Kim, M.H., Lee, J.M.: Prestrain-dependent viscoplastic damage model for austenitic stainless steel and implementation to ABAQUS user-defined material subroutine. Comput. Mater. Sci. **67**, 273–281 (2013). http://www.sciencedirect.com/science/article/pii/S0927025612005137. doi:10.1016/j.commatsci.2012.08.021

Klasztorny, M.: Coupled and uncoupled constitutive equations of linear elasticity and viscoelasticity of orthotropic materials. J. Theor. Appl. Mech. **46**(1), 3–20 (2008)

Li, Q.: Three dimensional numerical simulation of melt filling process in mold cavity with insets. Proc. Eng. **126**, 496–501 (2015)

Luo, G.M., Lee, Y.J.: Static crush experiments and simulations of laminated composite plates and shells with constrained layered damping. Compos. Struct. **85**(1), 64–69 (2008). http://www.sciencedirect.com/science/article/pii/S0263822307002413. doi:10.1016/j.compstruct.2007.10.023

Malerba, P., Guarnieri, F., Barros, J.: Aplicação da extensometria através dde strain gage: elatoboração de uma célula de carga com sistema de aquisiçao de dados computadorizado. In: VII Encontro Latino Americano de Pós-graduação, Universidade do Valo do Paraíba, São José dos Campos (2008)

Masuelli, M.A.: Introduction of Fibre-Reinforced Polymers—Polymers and Composites: Concepts, Properties and Processes. INTECH Open Access Publisher, Rijeka (2013)

Mertz, D.R.: Application of fiber reinforced polymer composites to the highway infrastructure. 503, Transportation Research Board (2003)

Nedjar, B.: An anisotropic viscoelastic fibre–matrix model at finite strains: continuum formulation and computational aspects. Comput. Methods Appl. Mech. Eng. **196**(9), 1745–1756 (2007)

Nedjar, B.: A time dependent model for unidirectional fibre-reinforced composites with viscoelastic matrices. Int. J. Solids Struct. **48**(16), 2333–2339 (2011)

Nguyen, T.D., Jones, R., Boyce, B.: Modeling the anisotropic finite-deformation viscoelastic behavior of soft fiber-reinforced composites. Int. J. Solids Struct. **44**(25), 8366–8389 (2007)

Östergren, A.: Prediction of residual stresses in injection molded parts. Dissertation, Chalmers University of Technology (2013)

Ozcelik, B., Kuram, E., Topal, M.M.: Investigation the effects of obstacle geometries and injection molding parameters on weld line strength using experimental and finite element methods in plastic injection molding. Int. Commun. Heat Mass Transf. **39**(2), 275–281 (2012). http://www.sciencedirect.com/science/article/pii/S0735193311002569. doi:10.1016/j.icheatmasstransfer.2011.11.012

Pandini, S., Pegoretti, A.: Time, temperature, and strain effects on viscoelastic Poisson's ratio of epoxy resins. Polym. Eng. Sci. **48**(7), 1434–1441 (2008). doi:10.1002/pen.21060

Papadogiannis, D., Lakes, R., Palaghias, G., Papadogiannis, Y.: Creep and dynamic viscoelastic behavior of endodontic fiber-reinforced composite posts. J. Prosthodont. Res. **53**(4), 185–192 (2009)

Park, S.: Analytical modeling of viscoelastic dampers for structural and vibration control. Int. J. Solids Struct. **38**(44–45), 8065–8092 (2001). http://www.sciencedirect.com/science/article/pii/S0020768301000269. doi:10.1016/S0020-7683(01)00026-9

Pettermann, H., Hüsing, J.: Modeling and simulation of relaxation in viscoelastic open cell materials and structures. Int. J. Solids Struct. **49**(19–20), 2848–2853 (2012). http://www.sciencedirect.com/science/article/pii/S0020768312001746, Proceedings of International Union of Theoretical and Applied Mechanics Symposium Mechanics of Liquid and Solid Foams. doi:10.1016/j.ijsolstr.2012.04.027.

Prabhakaran, S., Kumar, M.: Development of glass fiber reinforced polymer composite ceiling fan blade. Int. J. Eng. Res. Dev. **2**(3), 59–64 (2012)

Puso, M., Weiss, J.: Finite element implementation of anisotropic quasi-linear viscoelasticity using a discrete spectrum approximation. J. Biomech. Eng. **120**(1), 62–70 (1998)

Reese, S., Govindjee, S.: A theory of finite viscoelasticity and numerical aspects. Int. J. Solids Struct. **35**(26), 3455–3482 (1998)

Rios, T.J.A.: Revisão das dimensões da placa para extração dos corpos de prova. In: Grante/UFSC (2012)

Rosa, E.: Apostila de extensometria. In: Grante/UFSC (2004). http://grante.ufsc.br/download/Extensometria/SG-Apostila.pdf

Shoemaker, J.: Moldflow Design Guide: A Resource for Plastics Engineers. No. v. 10 in Moldflow Design Guide: A Resource for Plastics Engineers, Hanser (2006). https://books.google.com.br/books?id=ed2egd_3SGoC

Sonnenhohl, A.: Caracterização de material polimérico com reforço em fibras curtas de vidro. In: Grante/UFSC (2012)

Suchocki, C.: A quasi-linear viscoelastic rheological model for thermoplastics and resins. J. Theor. Appl. Mech. **51**(1), 117–129 (2013)

Tanasa, F., Zanoaga, M.: Fiber-reinforced polymer composites as structural materials for aeronautics. Sci. Res. Educ. Air Force, AFASES **2** (2013)

Tschoegl, N.: The Phenomenological Theory of Linear Viscoelastic Behavior: An Introduction. Springer, Berlin (1989). https://books.google.com.br/books?id=DJseAQAAIAAJ

Tschoegl, N., Knauss, W.G., Emri, I.: Poisson's ratio in linear viscoelasticity—a critical review. Mech. Time-Depend. Mater. **6**(1), 3–51 (2002). doi:10.1023/A:1014411503170

Vaz, M., Cardoso, E.L., Muñoz-Rojas, P.A., Carniel, T.A., Luersen, M.A., Tomiyama, M., da Silva, J.O., Stahlschmidt, J., Trentin, R.G.: Identification of constitutive parameters—optimization strategies and applications. Materialwiss. Werkstofftech. **46**(4–5), 477–491 (2015). doi:10.1002/mawe.201500423

Vélez-García, G., Mazahir, S., Wapperom, P., Baird, D.: Simulation of injection molding using a model with delayed fiber orientation. Int. Polym. Process. **26**(3), 331–339 (2011)

Wang, M., Shi, Y., Wang, Y.: Equivalent constitutive model of steel with cumulative degradation and damage. J. Constr. Steel Res. **79**, 101–114 (2012). http://www.sciencedirect.com/science/article/pii/S0143974X1200185X. doi:10.1016/j.jcsr.2012.07.028

Yang, B., Ouyang, J., Wang, F.: Simulation of stress distribution near weld line in the viscoelastic melt mold filling process. J. Appl. Math. **2013** (2013)

Yokoyama, T., Nakai, K.: Evaluation of in-plane orthotropic elastic constants of paper and paperboard. In: Proceeding of 2007 SEM Annual Conference & Exposition on Experimental and Applied Mechanics (2007)